

Ms. Ref. No.: EGY-D-15-00842R3**ACCEPTED MAY 17, 2016****Energy conversion under conjugate conduction, magneto-convection, diffusion and nonlinear radiation over a non-linearly stretching sheet with slip and multiple convective boundary conditions*****Md. Jashim Uddin*****American International University-Bangladesh, Banani, Dhaka 1213, BANGLADESH.****O. Anwar Bég****⁴Spray Research Group, Petroleum and Gas Engineering Division, Room G77, Newton Building, School of Computing, Science and Engineering (CSE), University of Salford, M54WT, UK,**Email: O.A.Beg@salford.ac.uk; goartoab@gmail.com.****Md. Nazir Uddin****Department of Mathematical Sciences, Ball State University, 2000 W University Avenue Muncie, INDIANA, IN 47306, USA.***Abstract**

Energy conversion under conduction, convection, diffusion and radiation has been studied for MHD free convection heat transfer of a steady laminar boundary-layer flow past a moving permeable non-linearly extrusion stretching sheet. The nonlinear Rosseland thermal radiation flux model, velocity slip, thermal and mass convective boundary conditions are considered to obtain a model with fundamental applications to real world energy systems. The Navier slip, thermal and mass convective boundary conditions are taken into account. Similarity differential equations with corresponding boundary conditions for the flow problem, are derived, using a scaling group of transformation. The transformed model is shown to be controlled by magnetic field, conduction-convection, convection-diffusion, suction/injection, radiation-conduction, temperature ratio, Prandtl number, Lewis number, buoyancy ratio and velocity slip parameters. The transformed non-dimensional boundary value problem comprises a system of nonlinear ordinary differential equations and physically realistic boundary conditions, and is solved numerically using the efficient Runge-Kutta-Fehlberg fourth fifth order numerical method, available in Maple17 symbolic software. Validation of results is achieved with previous simulations available in the published literature. The obtained results are displayed both in graphical and tabular form to exhibit the effect of the controlling parameters on the dimensionless velocity, temperature and concentration distributions. The current study has applications in high temperature materials processing utilizing magnetohydrodynamics, improved performance of MHD energy generator wall flows and also magnetic-microscale fluid devices.

Keywords: *Slip; Magneto-convective Free convection; Group analysis; Thermal and mass convective boundary conditions; Nonlinear radiation.*

** Corresponding author- Email: jashim_74@yahoo.com*

Nomenclature

a	velocity slip parameter (-)
$B(\bar{x})$	local magnetic field strength (T)
B_0	magnitude of magnetic field strength (T)
C	concentration (kgmol/m ³)
C_w	wall concentration (kgmol/m ³)
C_∞	ambient concentration (kgmol/m ³)
c_p	specific heat at constant pressure (J/kg K)
D	diffusion coefficient (m ² /s)
$f(\eta)$	dimensionless stream function (-)
fw	suction/injection parameter (-)
g	acceleration due to gravity (m/s ²)
h_f	heat transfer coefficient (W/m ² K)
h_m	mass transfer coefficient (m/s)
k	thermal conductivity (m ² /s)
k_1	Rosseland mean absorption coefficient (1/m)
L	characteristic length (m)
m	power law index of wall temperature and concentration (-)
M	magnetic field parameter (-)
N	radiation-conduction parameter (-)
$N_1(\bar{x})$	local velocity slip factor (s/m)
$(N_1)_0$	constant velocity slip factor (s/m)
Nc	convection-conduction parameter (-)
Nd	convection-diffusion parameter (-)
$Nu_{\bar{x}}$	local Nusselt number (-)
Pr	Prandtl number (-)
p	pressure (N/m ²)

q_m	wall mass flux (kg/s m^2)
q_w	wall heat flux (W/m^2)
q_r	component of radiative heat flux in \bar{y} - direction (W/m^2)
Le	Lewis number (-)
Ra	Rayleigh number (-)
$Sh_{\bar{x}}$	local Sherwood number (-)
T	fluid temperature (K)
T_w	wall temperature (K)
T_r	temperature ratio parameter (-)
T_∞	ambient temperature (K)
\bar{u}, \bar{v}	velocity components along the \bar{x} - and \bar{y} - axes (m/s)
\bar{u}_w	sheet velocity (m/s)
\bar{v}_w	transpiration velocity (m/s)
\bar{x}, \bar{y}	Cartesian coordinates along and normal to the sheet (m)

Greek

α	thermal diffusivity (m^2/s)
β_T	volumetric thermal expansion coefficient (1/K)
β_c	volumetric mass expansion coefficient (m^3/kgmol)
η	similarity variable (-)
$\theta(\eta)$	dimensionless temperature (-)
μ	viscosity of the fluid (Ns/m^2)
ν	kinematic viscosity of the fluid (m^2/s)
ρ	fluid density (kg/m^3)
σ_0	constant electric conductivity (S/m)
σ_1	Stefan-Boltzmann constant ($\text{W/m}^2\text{-K}^4$)
$\phi(\eta)$	dimensionless concentration (-)
ψ	stream function (-)

1. Introduction

The investigation of transport problems of viscous fluids associated with energy conversion passing a moving/stationary linearly/non-linearly extrusion surface is a relevant problem in many industrial processes including manufacture, drawing of plastics and rubber sheets, glass fiber and paper production, metal and polymer extrusion processes, cooling of metallic sheets and crystal growth, all of which utilize excessive energy input. It is necessary to cool the extrusion stretching sheet when the manufacturing process at high temperature. These flows need viscous fluids to make a good effect to control excessive temperature in the sheet. In addition, the fluids have been processed using a variety of supplementary effects (i.e. magnetic force, thermal/mass buoyancy and mass diffusion) for the problem, and effectively such systems constitute a conjugate energy conversion system which for optimization, requires both experimental and theoretical analysis. The rate of cooling/heating can be instrumental in determining the constitution of manufactured materials, in which a moving surface emerges from a slit and consequently, a boundary layer flow adjacent to the sheet is generated in the direction of the movement of the surface. Sakiadis [1] first investigated the boundary flow past a continuous solid surface, motivated by chemical processing applications. Thereafter Crane [2] studied the steady two- dimensional boundary layer flow of a viscous, incompressible fluid induced by a stretching sheet. As pointed out by Wang [3], there have been numerous analytical and numerical studies communicated on stretching/shrinking sheet flows. In this context we quote Pantokratoras [4], Van Gorder *et al.* [5], Hayat *et al.* [6] and Noghrehabadi *et al.* [7]. These studies have explored a wide range of thermophysical effects in stretching sheet transport phenomena. Yao *et al.* [8] reported on heat transfer of a viscous fluid flow past a stretching/shrinking sheet with a convective boundary condition. Bachok *et al.* [9] examined stagnation point flow toward a stretching/shrinking sheet

with a convective surface boundary condition. Some recent studies related to energy conversion are the paper of Elshafei [10] who studied natural convection heat transfer from a heat sink with hollow/perforated circular pin fins. Sertkaya et al. [11] presented pin-finned surfaces in natural convection. Bouaziz and Aziz [12] studied convective–radiative fin with temperature dependent thermal conductivity using double optimal linearization. Jang et al. [13] studied 3-D turbulent flow of venting flue gas using thermoelectric generator modules and plate fin heat sink. Torabi et al. [14] studied longitudinal fins of rectangular, trapezoidal and concave parabolic profiles with multiple nonlinearities.

Magnetohydrodynamics (MHD) has also grown into a significant area in many branches of engineering, not least in sustainable alternative energy generation. MHD involves the study of the influence of a magnetic field on the viscous flow of electrically-conducting fluids. It arises in magnetic materials processing, purification of crude oil, magnetohydrodynamic electrical power generation, manipulation of electro-conductive polymers, smart braking systems, external aerodynamic flow control for spacecraft and is also critical to TOKAMAK energy systems. In modern electromagnetic materials processing, MHD transport phenomena are exploited frequently in flows from continuously moving, stretching/shrinking, heated/cooled surfaces in a quiescent/moving free stream (Bataller [15]). MHD achieves excellent modification and control of magnetic fluids, which can be synthesized for specific applications including aerospace alloys (Beg *et al.* [16]). The manufactured materials are affected by the rate of stretching/shrinking, wall heat/mass transfer rates as well as by magnetic field strength (Chen [17]). Other uses of MHD include spacecraft landing gear systems (Holt [18]), deep space nuclear powered engines (Rashidi *et al.* [19]), magnetoplasma dynamic thrusters (Makinde and Bég [20]) and magnetic materials processing (Beg *et al.* [21]).

Thermal radiation heat transfer is important when the difference between the surface temperature and the free stream temperature is large and when the operating temperature is significantly high. Radiation plays an important role in controlling heat/mass as well as momentum transfer. It therefore exerts a substantial influence on the final constitution of materials during manufacturing, which can markedly impact on time to delivery by manufacturers. High temperature plasmas, cooling of nuclear reactors and glass production are some important applications of radiative heat transfer from a surface to conductive fluids. The effect of radiation on convective heat/mass transfer flow of both Newtonian and non-Newtonian fluids from either linearly or nonlinearly stretching/shrinking sheets has received extensive attention. Important studies in this regard include Chen [22], Noor *et al.* [23], Cortel [24], Misra and Sinha [25] and Hakeem *et al.* [26]. Previous investigators applied a linear Rosseland diffusion approximation for radiation which has limited accuracy when the temperature difference between the sheet and surrounding is very large. Very recently, Pantokratoras and Fang [27], Uddin *et al.* [28] and also Cortell [29] used the nonlinear Rosseland diffusion approximation to study radiative heat transfer. These studies showed that the nonlinear Rosseland flux model is valid for both small and large differences between surface temperature and ambient fluid temperature.

All of the previous investigators used uniform/variable concentration, uniform/variable mass flux or mass slip boundary conditions. They ignore *mass convective boundary conditions*. The idea of using mass convective boundary condition has been recently explored by Uddin *et al.* [30, 31].

Drying mechanism (naturally/artificially) in which heat and mass transfer occurs simultaneously is used in many agricultural and industrial sectors, e.g. food, wood, ceramic, pharmaceutical, and paper (Silva *et al.* [32]). The mass convective boundary condition is found to be most appropriate

to conduct an analysis of transport phenomena related to drying wet products artificially using hot air (Datta [33], Silva et al. [34]). The inclusion of this boundary condition makes the present study practically applicable. In the present article, we adopt this model and examine analytically and numerically the effect of thermal and mass convective boundary conditions on MHD free convective slip flow from a nonlinearly radiating stretching sheet. We develop similarity transformations via a one- parameter scaling group of transformations. The dimensionless conservation equations are derived as ordinary similarity differential equations for free convection flow of viscous incompressible fluid past a moving stretching sheet with thermal convective, mass convective and hydrodynamic slip boundary condition. The well-posed boundary value problem is solved using numerical quadrature provided in the symbolic code **Maple 17**. The effects of the emerging thermophysical and thermo-diffusive parameters on the flow, heat and mass transfer characteristics are explored graphically. Detailed interpretations of the solutions are documented.

2. Problem formulation

The two dimensional steady laminar free convective heat and mass transfer flow of a viscous, incompressible and electrically-conducting Newtonian fluid from a permeable moving nonlinear radiating stretching sheet is considered. The flow configuration and the coordinate system are presented in **Fig.1**. The sheet is orientated along the \bar{x} - axis. A magnetic field with variable strength $B(\bar{x}/L)$ is applied parallel to the \bar{y} axis *i.e. transverse to the sheet plane*. The magnetic Reynolds number is small enough to neglect induced magnetic field effects. It is also assumed that the external electric field is zero and the electric field due to polarization of charges is negligible. The pressure gradient, viscous and electrical dissipation are neglected. Applied magnetic field is also sufficiently weak to neglect Hall currents. The left surface of the sheet is heated by convection from a hot fluid at temperature T_f which provides a variable heat transfer coefficient, $h_f(\bar{x}/L)$. T_∞ denotes the ambient fluid temperature. It is assumed that

$T_f (> T_w > T_\infty)$. It is further assumed that the concentration at the left surface of the sheet is $C_f (> C_w > C_\infty)$ which provides a variable mass transfer coefficient $h_m(\bar{x}/L)$. C_w is the wall concentration and C_∞ is the ambient concentration. Thermophysical properties are assumed to be invariant except the density in the buoyancy terms. The field variables are the velocity components (\bar{u}, \bar{v}) , temperature, T , and concentration, C . Under these approximations, the mass, momentum, energy and species diffusion conservation equations in dimensional form are:

$$\frac{\partial \bar{u}}{\partial \bar{x}} + \frac{\partial \bar{v}}{\partial \bar{y}} = 0, \quad (1)$$

$$\bar{u} \frac{\partial \bar{u}}{\partial \bar{x}} + \bar{v} \frac{\partial \bar{u}}{\partial \bar{y}} = \frac{\mu}{\rho} \frac{\partial^2 \bar{u}}{\partial \bar{y}^2} - \frac{\sigma_0 B^2 (\bar{x}/L)}{\rho} \bar{u} + g\beta_T (T - T_\infty) (\bar{x}/L)^{-\left(\frac{3m+1}{3}\right)} + g\beta_C (C - C_\infty) (\bar{x}/L)^{-\left(\frac{3m+1}{3}\right)}, \quad (2)$$

$$\bar{u} \frac{\partial T}{\partial \bar{x}} + \bar{v} \frac{\partial T}{\partial \bar{y}} = \frac{k}{\rho c_p} \frac{\partial^2 T}{\partial \bar{y}^2} - \frac{1}{\rho c_p} \frac{\partial q_r}{\partial \bar{y}}, \quad (3)$$

$$\bar{u} \frac{\partial C}{\partial \bar{x}} + \bar{v} \frac{\partial C}{\partial \bar{y}} = D \frac{\partial^2 C}{\partial \bar{y}^2}. \quad (4)$$

The physical wall and far field boundary conditions imposed are (Ghiaasiaan [35]):

$$\begin{aligned} \bar{u} &= \bar{u}_w(\bar{x}/L) + \bar{u}_{\text{slip}}(\bar{x}/L), \bar{v} = \bar{v}_w(\bar{x}/L), -k \frac{\partial T}{\partial \bar{y}} = h_f(\bar{x}/L) [T_f - T(\bar{x}/L, 0)], \\ -D \frac{\partial C}{\partial \bar{y}} &= h_m(\bar{x}/L) [C_f - C(\bar{x}/L, 0)] \text{ at } \bar{y} = 0, \\ \bar{u} &\rightarrow 0, T \rightarrow T_\infty, C \rightarrow C_\infty \text{ as } \bar{y} \rightarrow \infty. \end{aligned} \quad (5)$$

Here $\bar{u}_w(\bar{x}) = \frac{\nu}{L} \left(\frac{\bar{x}}{L}\right)^{1/3}$ is sheet velocity, L is the characteristic length, $\bar{u}_{\text{slip}}(\bar{x}) = N_1(\bar{x}/L)\nu \frac{\partial \bar{u}}{\partial \bar{y}}$ is linear slip velocity, N_1 is velocity slip factor, ρ is density of the fluid, ν is the kinematic viscosity, k is the thermal conductivity, σ_0 is the fluid electric conductivity, $B(\bar{x}/L)$ is applied magnetic field, g denotes acceleration due to gravity, β_T designates volumetric coefficient of thermal expansion, β_C is the volumetric coefficient of concentration expansion, c_p is the specific heat at constant pressure, D is the mass (species) diffusivity, $\bar{v}_w(\bar{x}/L)$ is mass transfer velocity,

q_r is radiative heat flux, α is thermal diffusivity. The fluid is a gray, absorbing-emitting radiation but non-scattering medium (Cortell [29]). It is also assumed that the boundary layer is optically thick and the Rosseland approximation for radiation is valid. Thus for an optically thick

boundary layer (i.e. intensive absorption) the radiative heat flux is defined as $q_r = -\frac{4\sigma_1}{3k_1} \frac{\partial T^4}{\partial y}$,

where σ_1 ($= 5.67 \times 10^{-8} \text{ W/m}^2\text{K}^4$) is the Stefan-Boltzmann constant and k_1 (1/m) is the Rosseland mean absorption coefficient (Sparrow and Cess [36]).

2.1 Non-dimensionalization of Model

We introduce the following dimensionless variables in Eqns. (1)-(5):

$$x = \frac{\bar{x}}{L}, y = \frac{\bar{y}}{L} \text{Ra}^{1/4}, u = \frac{\bar{u}L}{\nu} \text{PrRa}^{-1/2}, v = \frac{\bar{v}L}{\nu} \text{PrRa}^{-1/4}, \theta = \frac{T-T_\infty}{\Delta T}, \phi = \frac{C-C_\infty}{\Delta C}, \quad (6)$$

$$\Delta T = T_f - T_\infty, \Delta C = C_f - C_\infty, \text{Ra} = \frac{g\beta_T(\Delta T)_0 L^3}{\nu\alpha}.$$

Introducing a dimensionless stream function ψ defined as:

$$u = \frac{\partial\psi}{\partial y} \text{ and } v = -\frac{\partial\psi}{\partial x}. \quad (7)$$

The continuity Eqn. (1) is satisfied identically and Eqns. (2)-(4) yield:

$$\frac{\partial\psi}{\partial y} \frac{\partial^2\psi}{\partial x\partial y} - \frac{\partial\psi}{\partial x} \frac{\partial^2\psi}{\partial y^2} = \text{Pr} \frac{\partial^3\psi}{\partial y^3} - \frac{\sigma_0 B^2(x)L^2}{\mu\text{Ra}^{1/2}} \text{Pr} \frac{\partial\psi}{\partial y} + \frac{g\beta_T(\Delta T)_0 x^{-1/3}L^3}{\nu\alpha\text{Ra}} \text{Pr} \left[\theta + \frac{\beta_C(\Delta C)_0}{\beta_T(\Delta T)_0} \phi \right], \quad (8)$$

$$\frac{\partial\psi}{\partial y} \frac{\partial\theta}{\partial x} + \frac{\partial\psi}{\partial y} \theta \frac{\partial}{\partial x} [\ln(\Delta T)] - \frac{\partial\psi}{\partial x} \frac{\partial\theta}{\partial y} = \frac{\partial^2\theta}{\partial y^2} + \frac{4}{3N} \frac{\partial}{\partial y} \left[\{1 + (T_r - 1)\theta\}^3 \frac{\partial\theta}{\partial y} \right], \quad (9)$$

$$\frac{\partial\psi}{\partial y} \frac{\partial\phi}{\partial x} + \frac{\partial\psi}{\partial y} \phi \frac{\partial}{\partial x} [\ln(\Delta C)] - \frac{\partial\psi}{\partial x} \frac{\partial\phi}{\partial y} = \frac{1}{\text{Le}} \frac{\partial^2\phi}{\partial y^2}. \quad (10)$$

The boundary conditions (5) now take the form:

$$\frac{\partial\psi}{\partial y} = x^{1/3} + \frac{\text{Ra}^{1/4}N_1(x)\nu}{L} \frac{\partial^2\psi}{\partial y^2}, -\frac{\partial\psi}{\partial x} = \frac{v_w L}{\alpha\text{Ra}^{1/4}}, \frac{\partial\theta}{\partial y} = -\frac{L}{\text{Ra}^{1/4}k} h_f(x)[1-\theta],$$

$$\frac{\partial\phi}{\partial y} = -\frac{L}{\text{Ra}^{1/4}D} h_m(x)[1-\phi] \text{ at } y=0, \quad (11)$$

$$\frac{\partial\psi}{\partial y} \rightarrow 0, \theta \rightarrow 0, \phi \rightarrow 0 \text{ as } y \rightarrow \infty.$$

Here $N = k k_1 / 4 \sigma_1 T_\infty^3$ the conduction-radiation parameter $Pr = \mu c_p / k$ is the Prandtl number, $Le = \alpha / D$ is the Lewis number, Ra is the Rayleigh number. It is further assumed that $\Delta T = (\Delta T)_0 x^m$, $\Delta C = (\Delta C)_0 x^m$, $(\Delta T)_0, (\Delta C)_0$ are constant reference temperature and concentration, m is the power law index of wall temperature and concentration (i.e. the flow is non-isothermal *and* non-isosolutal).

2.2 Search for Similarity using Symmetry Analysis

Following Uddin et al. [37], we select the following one-parameter continuous group of transformations:

$$\begin{aligned} \Gamma: x^* &= x e^{\varepsilon \alpha_1}, y^* = y e^{\varepsilon \alpha_2}, \psi^* = \psi e^{\varepsilon \alpha_3}, \theta^* = \theta e^{\varepsilon \alpha_4}, \phi^* = \phi e^{\varepsilon \alpha_5}, h_f^* = h_f e^{\varepsilon \alpha_6}, \\ v_w^* &= v_w e^{\varepsilon \alpha_7}, h_m^* = h_m e^{\varepsilon \alpha_8}, N_1^* = N_1 e^{\varepsilon \alpha_9}, B^{*2} = B^2 e^{\varepsilon \alpha_{10}}. \end{aligned} \quad (12)$$

Here ε is the parameter of the group and α_i ($i=1,2,\dots,10$) are arbitrary real numbers. We seek the values of α_i such that the form of the Eqns. (8)-(11) is invariant under the transformation group. This transforms the variables from $(x, y, \psi, \theta, \phi, h_f, h_m, v_w, N_1, B^2)$ to $(x^*, y^*, \psi^*, \theta^*, \phi^*, h_f^*, h_m^*, v_w^*, N_1^*, B^{*2})$. Substituting Eqn. (12) into Eqns. (8)-(11), equating powers of e and hence solving the resulting equations, we arrive at:

$$\alpha_4 = \alpha_5 = 0, \quad \alpha_1 = 3\alpha_2, \quad \alpha_3 = 2\alpha_2, \quad \alpha_{10} = -2\alpha_2, \quad \alpha_6 = \alpha_7 = \alpha_8 = -\alpha_2, \quad \alpha_9 = \alpha_2 \quad (13)$$

With these values of α , the set of transformations Γ then reduces to :

$$\begin{aligned} \Gamma: x^* &= x e^{3\varepsilon \alpha_2}, y^* = e^{\varepsilon \alpha_2} y, \psi^* = \psi e^{2\varepsilon \alpha_2}, \theta^* = \theta, \phi^* = \phi, h_f^* = h_f e^{-\varepsilon \alpha_2}, \\ v_w^* &= v_w e^{-\varepsilon \alpha_2}, h_m^* = h_m e^{-\varepsilon \alpha_2}, N_1^* = N_1 e^{\varepsilon \alpha_2}, B_1^{*2} = B_1^2 e^{-\varepsilon 2\alpha_2}. \end{aligned} \quad (14)$$

We now seek the absolute invariants under this group of transformations. To determine the absolute invariant, we expand transformations (14) as a Taylor series retaining the terms up to the first degree and neglecting higher powers of ε . This yields the following characteristic equations:

$$\frac{dx}{3x} = \frac{dy}{y} = \frac{d\psi}{2\psi} = \frac{d\theta}{0} = \frac{d\phi}{0} = \frac{dh_f}{-h_f} = \frac{dv_w}{-v_w} = \frac{dh_m}{-h_m} = \frac{dN_1}{N_1} = \frac{dB^2}{-2B^2}. \quad (15)$$

2.3 Similarity Transformations

Solving (15), we have the following similarity transformations (absolute invariants)

$$\begin{aligned} \eta &= yx^{-1/3}, \quad \psi = x^{2/3}f(\eta), \quad \theta = \theta(\eta), \quad \phi = \phi(\eta), \quad h_f = h_{f_0}x^{-1/3}, \quad h_m = h_{m_0}x^{-1/3}, \\ v_w &= v_{w_0}x^{-1/3}, \quad N_1 = N_{1_0}x^{1/3}, \quad B^2 = B_0^2x^{-2/3}. \end{aligned} \quad (16)$$

Here $h_{f_0}, v_{w_0}, h_{m_0}, N_{1_0}, B_0^2$ are constant heat transfer coefficient, constant transpiration (wall lateral mass flux) velocity, constant mass transfer coefficient, constant velocity slip factor, constant transverse magnetic field. $f(\eta), \theta(\eta), \phi(\eta)$ are the dimensionless stream function, temperature and concentration respectively.

2.4 Similarity Differential Equations

Using Eqn. (16), Eqns. (8) - (11) reduce to the following coupled, nonlinear similarity equations:

$$f''' + \frac{1}{3Pr} (2ff'' - f'^2) - Mf' + \theta + Nr\phi = 0, \quad (17)$$

$$\theta'' + \frac{4}{3N} \left[\{1 + (T_r - 1)\theta\}^3 \theta' \right] + \left[\frac{2}{3} f\theta' - mf'\theta \right] = 0, \quad (18)$$

$$\frac{1}{Le} \phi'' + \left[\frac{2}{3} f\phi' - mf'\phi \right] = 0, \quad (19)$$

$$\begin{aligned} f(0) &= fw, \quad f'(0) = 1 + af''(0), \quad \theta'(0) = -Nc[1 - \theta(0)], \quad \phi'(0) = -Nd[1 - \phi(0)], \\ f'(\infty) &= \theta(\infty) = \phi(\infty) = 0. \end{aligned} \quad (20)$$

Here $M = \sigma L^2 B_0^2 / \mu \sqrt{Ra}$ (magnetic field parameter), $Nr = \beta_c (\Delta C)_0 / \beta_T (\Delta T)_0$ (buoyancy ratio), $Nc = Lh_{f_0} / Ra^{1/4} k$, (convection-conduction parameter), $Nd = Lh_{m_0} / DRa^{1/4}$ (convection-diffusion parameter), $fw = -3Lv_{w_0} / 2Ra^{1/4} a$ (suction/injection i.e. wall transpiration parameter), $fw > 0$ for suction, $fw < 0$ for injection and $fw = 0$ for solid sheet), $a = N_{1_0} \nu Ra^{1/4} / L$ (velocity slip),

$T_r = \frac{T_f}{T_\infty}$ (temperature ratio). We note that when $Nc=Nd \rightarrow \infty$, $M=Nr=a=0$, $Pr = 1$, the boundary value problem retracts to the simpler model investigated by Hsiao (Hsiao [38]).

3. Physical Quantities

In sheet materials processing and near wall MHD energy generator flows, important design quantities are the skin friction $C_{f\bar{x}}$, the local Nusselt number $Nu_{\bar{x}}$ and the local Sherwood number $Sh_{\bar{x}}$ can be found from the following definitions:

$$C_{f\bar{x}} = \frac{\tau_w}{\rho \bar{u}_w^2}, \quad Nu_{\bar{x}} = \frac{\bar{x} q_w}{k(T_f - T_\infty)}, \quad Sh_{\bar{x}} = \frac{\bar{x} q_m}{D(C_f - C_\infty)}, \quad (21)$$

where τ_w , q_w , q_m are the wall shear stress, the wall heat and the wall mass fluxes, respectively, and are defined as

$$\tau_w = \mu \left(\frac{\partial \bar{u}}{\partial \bar{y}} \right)_{\bar{y}=0}, \quad q_w = -k \left[1 + \frac{16\sigma_1}{3k_1 k} T^3 \right] \left(\frac{\partial T}{\partial \bar{y}} \right)_{\bar{y}=0}, \quad q_m = -D \left(\frac{\partial C}{\partial \bar{y}} \right)_{\bar{y}=0}. \quad (22)$$

Using Eqns. (6), (16), (22), we have from Eqn. (21)

$$Re_{\bar{x}}^{-1/2} Pr^{1/2} C_{f\bar{x}} = -f'(0), \quad Re_{\bar{x}}^{1/2} Pr^{-1/2} Nu_{\bar{x}} = - \left[1 + \frac{4}{3N} \left[\{1 + (T_r - 1)\theta\}^3 \theta' \right]' \right] \theta'(0), \quad Re_{\bar{x}}^{1/2} Pr^{-1/2} Sh_{\bar{x}} = -\phi'(0), \quad (23)$$

where $Re_{\bar{x}} = \frac{\bar{u} \bar{x}}{\nu}$ is the local Rayleigh number.

4. Numerical Solution by Maple 17

With the application of a scaling group of transformations for the governing boundary layer equations and associated boundary conditions, the two independent variables are reduced by one. Consequently the governing equations reduce to a system of dimensionless nonlinear ordinary differential equations and associated boundary conditions. The nonlinear two-point boundary value problem is solved using **MAPLE17** which uses the Runge–Kutta–Fehlberg fourth-fifth

order numerical algorithm (**RKF45**). This approach has been extensively implemented in a diverse array of nonlinear multi-physical flow problems in chemical and materials engineering sciences including entropy minimization in magnetic materials processing [39], viscoelastic petroleum flows [40], annular magnetohydrodynamics [41], nano-structural mechanics [42], nanofluid convection flows [43, 44] and thermo-capillary convection [45]. The robustness and stability of this numerical method is therefore well established. A Runge–Kutta–Fehlberg fourth-fifth order numerical algorithm (**RKF45**) is employed, available in the symbolic computer software **Maple 17**. The **RKF45** algorithm is adaptive since it adjusts the quantity and location of grid points during iteration and thereby constrains the local error within acceptable specified bounds. In the current problem, the asymptotic boundary conditions given in Eqn. (20) are replaced by a finite value 12. The choice of infinity must be selected judiciously to ensure that all numerical solutions approached to the asymptotic values correctly. The selection of sufficiently large value for infinity is imperative for maintaining desired accuracy in boundary layer flows, and is a common pitfall encountered in numerous studies. The stepping formulae used to solve Eqns. (17)-(19) under conditions (20) via fifth-fourth order Runge-Kutta-Fehlberg algorithms are given below [46]:

$$k_0 = f(x_i, y_i), \quad (24)$$

$$k_1 = f\left(x_i + \frac{1}{4}h, y_i + \frac{1}{4}hk_0\right), \quad (25)$$

$$k_2 = f\left(x_i + \frac{3}{8}h, y_i + \left(\frac{3}{32}k_0 + \frac{9}{32}k_1\right)h\right), \quad (26)$$

$$k_3 = f\left(x_i + \frac{12}{13}h, y_i + \left(\frac{1932}{2197}k_0 - \frac{7200}{2197}k_1 + \frac{7296}{2197}k_2\right)h\right), \quad (27)$$

$$k_4 = f\left(x_i + h, y_i + \left(\frac{439}{216}k_0 - 8k_1 + \frac{3860}{513}k_2 - \frac{845}{4104}k_3\right)h\right), \quad (28)$$

$$k_5 = f \left(x_i + \frac{1}{2}h, y_i + \left(-\frac{8}{27}k_0 + 2k_1 - \frac{3544}{2565}k_2 + \frac{1859}{4104}k_3 - \frac{11}{40}k_4 \right) h \right), \quad (29)$$

$$y_{i+1} = y_i + \left(\frac{25}{216}k_0 + \frac{1408}{2565}k_2 + \frac{2197}{4104}k_3 - \frac{1}{5}k_4 \right) h, \quad (30)$$

$$z_{i+1} = z_i + \left(\frac{16}{135}k_0 + \frac{6656}{12825}k_2 + \frac{28561}{56430}k_3 - \frac{9}{50}k_4 + \frac{2}{55}k_5 \right) h, \quad (31)$$

Here y denotes fourth-order Runge-Kutta phase and z is the fifth-order Runge-Kutta phase. An estimate of the error is achieved by subtracting the two values obtained. If the error exceeds a specified threshold, the results can be re-calculated using a smaller step size. The approach to estimating the new step size is shown below:

$$h_{\text{new}} = h_{\text{old}} \left(\frac{\varepsilon h_{\text{old}}}{2 |z_{i+1} - y_{i+1}|} \right)^{1/4} \quad (32)$$

5. Presentation of Results

In order to assess the accuracy of the numerical method, we have compared the local skin friction coefficient i.e. $f''(0)$, with the previously published data of Cortell [29], for selected values of suction/injection parameter fw and $Nc \rightarrow \infty$ with $M = a = 0$. The comparison is shown in **Table 1**, and is found to be in excellent agreement. This degree of closeness vouches for the high accuracy of the present computational scheme. The computational solutions are depicted in **Figs. 2-14** for the influence of selected parameters on the flow, heat and mass transfer characteristics.

In the graphs presented the following default data is employed for the governing thermophysical parameters: $Pr = \mu c_p / k = 6.8$ (high viscosity fluids e.g. polymers, for which momentum diffusivity exceeds thermal diffusivity), $Le = \alpha / D = 5$ (Lewis number defines the ratio of

thermal diffusivity to mass (nanoparticle species) diffusivity. It is used to characterize fluid flows where there is simultaneous heat and mass transfer by convection. For $Le > 1$, thermal diffusion rate exceeds species diffusion rate), $Nr = \beta_c (\Delta C)_0 / \beta_T (\Delta T)_0 = 0.1$ (thermal buoyancy force exceeds greatly the species buoyancy force), $m = 1$ (non-isothermal, non-iso-solutal case), $a = N_1 \nu Ra^{1/4} / L = 1$ (strong velocity slip), $M = \sigma L^2 B_0^2 / \mu \sqrt{Ra} = M = 0.5$ (weak magnetic field), $Nc = L h_{f_0} / Ra^{1/4} k = 0.5$ (conduction exceeds convection heat transfer), $Nd = L h_{f_0} / DRa^{1/4} = 0.5$ (diffusion exceeds convection), $N = k k_1 / 4\sigma_1 T_\infty^3 = 10$ (thermal conduction exceeds thermal radiation). $T_r = \frac{T_f}{T_\infty} = 2$ (high temperature ratio). This data is realistic for materials processing systems and also certain MHD energy generator channel flows in the wall vicinity.

Fig.2 shows a sample computation for the evolution of the dimensionless velocity, temperature and concentration. This clearly establishes the nature of the velocity, temperature and concentration behavior from the wall, transverse to the sheet into the boundary layer. The monotonic decay of all flow characteristics from the sheet surface is evident. Velocity is observed to be greater than temperature and this in turn exceeds concentration. This indicates physically that the momentum boundary layer thickness exceeds thermal boundary layer thickness, which in turn is greater than concentration boundary layer thickness. The stable and asymptotically smooth nature of the profiles in the free stream, also confirms that with all thermophysical parameters invoked (i.e. radiation, mass, momentum, thermal slip, and wall injection) the correct behavior is computed for all the variables. Flow reversal is not induced (negative values do not arise for velocity), and no temperature or concentration overshoots are observed. Fig. 2 corresponds to very weak thermal radiation present ($N = k k_1 / 4\sigma_1 T_\infty^3$ i.e. conduction-radiation parameter = 10 i.e. *conduction* \gg *radiation*, in fig. 2) and more details of stronger radiative flux are elucidated in due course.

Figs. 3–5, show the effects of radiation-conduction (N) and suction/injection (fw) parameters on the dimensionless velocity, temperature and concentration distributions. The dimensionless velocity (fig. 3) and temperature (fig. 4) magnitudes evidently are both strongly reduced with increasing N . $N = k k_1 / 4\sigma_1 T_\infty^3$ and embodies the relative contribution of thermal conduction heat

transfer to radiative heat transfer. This parameter, also known as the Rosseland-Boltzmann number (Bég et al. [45]) arises in the augmented thermal diffusion term, $\frac{4}{3N} \left\{ 1 + (T_r - 1)q^3 \right\} q' / \eta$ in the normalized energy conservation equation (18). Clearly this parameter is a reciprocal. As N increases the contribution of thermal radiation decreases and thermal conduction increases. As $N \rightarrow \infty$ thermal radiative flux contribution will vanish. As $N \rightarrow 0$, thermal conduction contribution will vanish. Effectively as N increases, the ratio $(4/3 N)$ will be reduced. The temperature in the boundary layer will therefore be decreased (lower radiative flux) and thermal boundary layer thickness will also be reduced. Via coupling of the energy field with the momentum conservation equation (17), an increase in N will decelerate the boundary layer flow leading to a thickening of momentum (hydrodynamic) boundary layer thickness. Similar trends of velocity and temperature profiles have been observed by Pal et al. [48]. The general trends for radiative effects computed are also corroborated in actual materials processing operations, as described by Viskanata [49]. Fig 5 demonstrates that the concentration magnitude increases as N increases for both permeable ($f_w \neq 0$) and impermeable ($f_w = 0$) plates. Species diffusion is thereby clearly accentuated with a reduction in radiative heat flux, and this also leads to a thickening in the species (concentration) boundary layer thickness. In figs. 3-5, an increase in injection ($f_w < 0$) consistently enhances velocity, temperature and species concentration. The lateral mass flux of fluid into the boundary layer regime is enhanced with injection (blowing). This boosts momentum and also aids in thermal and species diffusion, leading to *thinner* velocity boundary layers and *thicker* thermal and concentration boundary layers. The reverse effect is induced with suction ($f_w > 0$) which causes the momentum boundary layer to adhere more strongly to the sheet surface, inhibits momentum development and simultaneously impedes heat and mass (species) diffusion. Evidently both radiation heat flux and wall transpiration exert a profound influence on the flow characteristics and both effects are extremely potent in materials processing operations. Asymptotically smooth distributions are achieved into the free stream, in all these figures, showing that an adequately large infinity boundary condition has been specified in the **Maple** routine **dsolve**.

Figs. 6–8, display the effects of velocity slip parameter on the dimensionless velocity, temperature and concentration distributions in the presence of suction/injection parameter

($fw \neq 0$) and in the absence of suction/injection parameter ($fw = 0$) respectively. It is observed that the velocity distributions decrease with increase in “a” for both cases ($fw \neq 0$) and ($fw = 0$) whilst temperature and concentration increase. Greater velocity slip at the wall therefore inhibits momentum diffusion in the boundary layer, in particular close to the sheet. Further into the boundary layer, the effect is progressively decreased. Since both thermal and species diffusion are exacerbated with greater wall velocity slip at the sheet, this will manifest in thicker species and thermal boundary layers. The dominant effect of wall velocity slip is generally confined to the near-wall zone and in practical materials sheet processing; the hydrodynamic slip effect is expected to be most dominant near the sheet surface. This can of course be exploited to achieve some modification of for example polymer sheet properties in that region, whereas the influence throughout the sheet, transverse to the wall, will be minimal. It is also interesting to note that while all three velocity, temperature and concentration distributions exhibit monotonic decays from the sheet surface to the free stream, the rate of descent of the concentration profiles is much sharper than for velocity and temperature profiles. The species diffusion field is evidently much more sensitive to an increase in transverse coordinate value (η) than the momentum and thermal fields. Modification of sheet properties in terms of species distribution therefore requires a faster and more pronounced action than the velocity and thermal characteristics of sheets.

Fig. 9, shows the effects of the convection-diffusion parameter ($Nd = Lh_{f_0}/DRa^{1/4}$) on the dimensionless concentration distributions in the presence of suction/injection parameter ($fw \neq 0$) and in the absence of suction/injection parameter ($fw = 0$). The parameter Nd also represents the mass Biot number. The dimensionless concentration distributions are elevated by increasing mass Biot number for both cases ($fw \neq 0$) and ($fw = 0$). The mass Biot number Nd , is the ratio of the internal solutal resistance of a solid to the boundary layer thermal resistance. The parameter Nd features in the boundary conditions (20) relating to the species gradient at the sheet i.e. $\phi(0) = -Nd [1 - \phi(0)]$. When $Nd = 0$ (i.e. without mass Biot number) the left side of the plate with high concentrated fluid is *totally insulated*, the internal solutal resistance of the plate is extremely high and *no convective heat transfer* to the cold fluid on the right side of the plate takes place. Fig. 8 also confirms the positive influence of injection on momentum, heat and thermal diffusion and the counteracting influence of suction ($fw > 0$) on these characteristics.

Strong retardation of the flow accompanies increasing wall suction, whereas significant acceleration is associated with increasing injection. Thermal and concentration boundary layer thicknesses are also enhanced with injection whereas they are reduced with suction.

Figs. 10-12, show the effects of magnetic field parameter ($M = \sigma L^2 B_0^2 / \mu \sqrt{Ra}$) and wall transpiration parameter (fw) on the dimensionless velocity, temperature and concentration distributions. Magnetic field arises only in the Lorentzian body force term, $-Mf'$, in the momentum boundary layer equation (17). This is a linear force generated by the application of a transverse magnetic field to the sheet flow regime, and acts perpendicular to the direction of the magnetic field, B_0 , i.e. along the negative \bar{x} -axis (fig. 1). The Lorentz magnetohydrodynamic force is a drag force therefore resisting momentum development and impeding the boundary layer flow. In the absence of the magnetic field, $M = 0$ (electrically non-conducting fluid) and magnetohydrodynamic drag vanishes. The dimensionless velocity is therefore a maximum for this scenario (fig. 10). With increasing M , there is a strong deceleration in the flow and momentum boundary layer thickness is enhanced. Conversely the dimensionless temperatures in the boundary layer are enhanced with increasing M (fig. 11) and this is attributable to the dissipation in the supplementary work expended in dragging the fluid against the action of the magnetic field. This extra work is dissipated as thermal energy which heats the boundary layer, elevates temperatures and enhances thermal boundary layer thickness. A similar but less dramatic effect is observed for the concentration field, (fig. 12) where species concentration is also found to be elevated with increasing magnetic field, also leading to a thickening of the concentration boundary layer. The magnetohydrodynamic effect therefore aids thermal and species diffusion whereas it opposes momentum development. The magnetic field effect is therefore a powerful mechanism for modifying flow characteristics during sheet materials processing. We further note that fig. 9 presents solutions for the weakly non-isothermal and non-iso-solutal case, $m = 0.5$, whereas other graphs presented correspond to a stronger non- isothermal and non-iso-solutal case ($m=1$). Figs. 10-12 also verify the earlier observations in so far as wall transpiration is concerned, namely that the flow is accelerated and temperatures and concentration values are increased with wall injection ($fw < 0$), whereas they are stifled with wall suction ($fw > 0$).

Figs. 13-14, show the effects of temperature ratio (T_r) and wall mass flux parameter (f_w) on the dimensionless velocity and temperature distributions. It is observed that the velocity (fig. 13) as well as temperature (fig. 14) distributions increases with an increase in temperature ratio parameter. Momentum boundary layer thickness is reduced and thermal boundary layer thickness is enhanced with increasing T_r values. The enhancement is however more dramatic, as anticipated, for the temperature field, since T_r arises solely in the augmented thermal diffusion term, $\frac{4}{3N} \left\{ 1 + (T_r - 1)q^3 \right\} q / \frac{\partial \theta}{\partial \eta}$ in the energy equation (18). Via coupling of the energy and momentum equation (17), the velocity field is indirectly influenced with the temperature ratio parameter and experiences a lesser modification as a result. Figs. 13, 14 also again demonstrate the assistive effect of wall transpiration on heat, mass and momentum characteristics and the opposing effect of suction. Smooth convergence of the velocity and temperature fields in the free stream is again achieved (as in all other plots), testifying to the selection of an appropriately large infinity boundary condition in the numerical computations performed with **Maple 17 dsolve** routines.

6. Conclusions

A theoretical and computational study has been presented for steady two-dimensional laminar free convective radiative magnetohydrodynamic heat, mass and momentum transfer in viscous flow from a non-isothermal and non-isosolutal continuously moving sheet. Similarity differential equations with corresponding and boundary conditions for the transport equations have been obtained via a robust scaling group transformation procedure. The nonlinear ordinary differential boundary value problem is shown to be controlled by an extensive range of parameters, including magnetic body force parameter (M), conduction-convection parameter (N_c), convection-diffusion parameter (N_d), non-isothermal/non-iso-solutal power-law index (m), lateral mass flux (transpiration) parameter (f_w), radiation-conduction parameter (N), temperature ratio (T_r), Prandtl number (Pr), Lewis number (Le), buoyancy ratio (N_r) and velocity slip (a). Numerical solutions have been obtained using **dsolve** command in **Maple 17** symbolic software, for selected values of certain parameters. The numerical methodology has been benchmarked for the non-magnetic case, in the absence of wall velocity slip with the previously published data of Cortell [24], for selected

values of suction/injection parameter (f_w) demonstrating excellent correlation. The present computations have shown that:

- (i) Increasing magnetic field enhances temperatures and concentrations whereas it depresses velocity magnitudes (although flow reversal is not induced).
- (ii) Increasing velocity slip at the wall reduces flow velocity whereas it enhances temperature and concentration.
- (iii) Increasing radiation-conduction parameter (corresponding to a reduction in thermal radiative flux contribution) generates flow deceleration and a decrease in temperatures, whereas it elevates concentration magnitudes.
- (iv) Increasing wall suction ($f_w > 0$) retards the boundary layer flow and depresses temperatures and concentration values, whereas increasing injection (blowing at the sheet) manifests in the opposite effect.
- (v) Increasing convection-diffusion parameter (N_d) enhances concentration magnitudes.
- (vi) Increasing temperature ratio (T_r) slightly accelerates the flow but strongly enhances temperatures through the boundary layer.

The present simulations have been confined to Newtonian viscous fluids. Future investigations will study velocity slip effects for a range of rheological materials e.g. viscoelastic liquids (Bég *et al.* [46]), micropolar biopolymers (Bég *et al.* [47]) and power-law shear thinning/thickening nanofluids (Uddin *et al.* [37]), and will be communicated imminently.

References

- [1] Sakiadis BC. Boundary-layer behavior on a continuous solid surface: II- The boundary layer on a continuous flat surface. *AIChE J* 1961; 7:221-225.
- [2] Crane LJ. Flow past a stretching plate. *J Appl Math and Phy (ZAMP)* 1970; 21:590-595.
- [3] Wang CY. Review of similarity stretching exact solutions of the Navier-Stokes equations. *Eur J Mech B/Fluids* 2011; 30:475-479.
- [4] Pantokratoras A. Study of MHD boundary layer flow over a heated stretching sheet with variable viscosity: a numerical reinvestigation. *Int J Heat and Mass Transfer* 2008; 51: 104-110.
- [5] Van Gorder RA, Sweet E, Vajravelu K. Nano-boundary layers over stretching surfaces. *Commun Nonl Sci Numer Simul* 2010; 15:1494–1500.
- [6] Hayat T, Qasim M, Mesloub S. MHD flow and heat transfer over permeable stretching sheet with slip conditions. *Int J. Numer Meth in Fluids* 2011; 66: 963-975.
- [7] Noghrehabadi A, Pourrajab R, Ghalambaz M. Effect of partial slip boundary

- condition on the flow and heat transfer of nanofluids past stretching sheet prescribed constant wall temperature. *Int J Therm Sci* 2012;54: 253-261.
- [8] Yao S, Fang T, Zhong Y. Heat transfer of a generalized stretching/shrinking wall problem with convective boundary conditions. *Commun Nonl Sci Numer Simulat* 2011;16: 752–760.
- [9] Bachok N, Ishak A, Pop, I. Stagnation point flow toward a stretching/shrinking sheet with a convective surface boundary condition. *J Franklin Ins* 2013; 350:2736-2744.
- [10] Elshafei EAM. Natural convection heat transfer from a heat sink with hollow/perforated circular pin fins. *Energy* 2010; 35:2870-7.
- [11] Sertkaya AA, Bilir S, Kargıcı S. Experimental investigation of the effects of orientation angle on heat transfer performance of pin-finned surfaces in natural convection. *Energy* 2011; 36:1513-7.
- [12] Bouaziz MN, Aziz A. Simple and accurate solution for convective-radiative fin with temperature dependent thermal conductivity using double optimal linearization. *Energy Convers Manage* 2010;51:2776-82.
- [13] Jang Jiin-Yuh, Tsai Ying-Chi, Wu Chan-Wei. A study of 3-D numerical simulation and comparison with experimental results on turbulent flow of venting flue gas using thermoelectric generator modules and plate fin heat sink. *Energy* 1 May 2013;53:270-81.
- [14] Torabi Mohsen, Aziz Abdul, Zhang Kaili. A comparative study of longitudinal fins of rectangular, trapezoidal and concave parabolic profiles with multiple nonlinearities. *Energy* 1 March 2013; 51:243-56.
- [15] Bataller RC, Magnetohydrodynamic flow and heat transfer of an upper-convected Maxwell fluid due to a stretching sheet. *Fluid Dynamics & Mat Proces* 2011;7:153-174.
- [16] Beg OA, Bakier AY, Prasad VR. Numerical study of free convection magnetohydrodynamic heat and mass transfer from a stretching surface to a saturated porous medium with Soret and Dufour effects. *Comput Mat Sci* 2009; 46:57-65.
- [17] Chen C.H. Mixed convection cooling of a stretching sheet in the presence of a magnetic field for manufacturing processes. *Key Eng Mat* 2010; 419/420:353-356.
- [18] Holt AC. Electromagnetic braking for Mars spacecraft, In: *AIAA-1986-1588 ASME, SAE, and ASEE, 22nd, Joint propulsion conference, Huntsville, Alabama, USA, June 16–18 (1986)*.
- [19] Rashidi MM, Bég OA, Mehr NF, Rostami B. Second law analysis of hydromagnetic flow from a stretching rotating disk: DTM-Pade simulation of novel nuclear MHD propulsion systems. *Frontiers in Aerospace Eng* 2103; 2:29-38.
- [20] Makinde OD, Bég OA. On inherent irreversibility in a reactive hydromagnetic channel flow. *J Therm Sci* 2010;19:72-79.
- [21] Bég OA, Zueco J, Ghosh SK, Heidari A. Unsteady magnetohydrodynamic heat transfer in a semi-infinite porous medium with thermal radiation flux: analytical and numerical study. *Adv in Numer Anal* 2011; 2011:1-17.
- [22] Chen TM. Radiation effects on magnetohydrodynamic free convection flow. *AIAA J. Thermophysics Heat Transfer* 2008; 22:125-128.
- [23] Noor NFM, Abbasbandy S, Hashim I. Heat and mass transfer of thermophoretic MHD flow over an inclined radiate isothermal permeable surface in the presence of heat source/sink. *Int J Heat Mass Transfer* 2012; 55: 2122–2128.
- [24] Cortell R. Heat transfer in a fluid through a porous medium over a permeable stretching surface with thermal radiation and variable thermal conductivity. *Can J of Chem Eng* 2011; 90 (5): 1347–1355.

- [25] Misra JC, Sinha A. Effect of thermal radiation on MHD flow of blood and heat transfer in a permeable capillary in stretching motion. *Heat and Mass Transfer* 2013;48:1-12.
- [26] Hakeem KA, Ganesh NV, Ganga B. Effect of heat radiation in a Walter's liquid B fluid over a stretching sheet with non-uniform heat source/sink and elastic deformation. *J. King Saud Uni - Eng Sci* 2014; 4:913–922.
- [27] Pantokratoras A, Fang T. Sakiadis flow with nonlinear Rosseland thermal radiation. *Phy Scr* 2013; 87:015703 (5pp).
- [28] Uddin MJ, Bég OA, Ismail AIM. Radiative convective nanofluid flow past a stretching/shrinking sheet with slip boundary conditions. *AIAA J Heat Transfer*, doi: 10.2514/1.
- [29] Cortell R. Fluid flow and radiative nonlinear heat transfer over a stretching sheet. *J of King Saud Uni-Sci* 2014; 26: 161-167.
- [30] Uddin, MJ, Bég, OA, Ismail, AIM. Mathematical modelling of radiative hydromagnetic thermosolutal nanofluid convection slip flow in saturated porous media, *Math Prob in Eng*, 2014, 2014, Article ID 179172, 11 pages.
- [31] Uddin MJ, Khan WA, Ismail AIM. G-jitter induced magnetohydrodynamics flow of nanofluid with constant convective thermal and solutal boundary conditions. *PLoS ONE* 2015, 10(5): e0122663.
- [32] W.P. Silva, J.W. Precker, C.M.D.P.S. Silva, J.P. Gomes, Determination of effective diffusivity and convective mass transfer coefficient for cylindrical solids via analytical solution and inverse method: Application to the drying of rough rice. *J. of Food Eng.* 98(2010)302-308.
- [33] A.K. Datta, *Biological and Bioenvironmental Heat and Mass Transfer*, Marcel Dekker, New York, USA, 2002.
- [34] Silva, C.D.D.D, Silva W.P., FARIAS, V.D., Gomes, J.P, Effective diffusivity and convective mass transfer coefficient during the drying of bananas. *Eng. Agríc., Jaboticabal* 32(2012)342-353.
- [35] Ghiaasiaan SM. *Convective Heat and Mass Transfer*. Cambridge University Press Cambridge, New York, USA (2011).
- [36] Sparrow EM, Cess RD. *Radiation Heat Transfer*. Hemisphere, Washington (Chaps. 7 & 10) (1978).
- [37] Uddin MJ, Ferdows M, Bég OA. Group analysis and numerical computation of magneto-convective non-Newtonian nanofluid slip flow from a permeable stretching sheet. *Appl Nanosci* 2014; 4:897-910.
- [38] Hsiao KL. Energy conversion conjugate conduction–convection and radiation over non-linearly extrusion stretching sheet with physical multimedia effects. *Energy* 2013, 59: 494-502.
- [39] Makinde, OD, Bég OA. On inherent irreversibility in a reactive hydromagnetic channel flow, *J. Therm Sci* 2010, 19:1-8.
- [40] Bég, OA, Makinde OD. Viscoelastic flow and species transfer in a Darcian high-permeability channel, *Petro Sci and Eng* 2011, 76:93–99.
- [33] Makinde OD, Bég, OA, Takhar HS. Magnetohydrodynamic viscous flow in a rotating porous medium cylindrical annulus with an applied radial magnetic field, *Int. J. Appl Math and Mec* 2009, 5:68-81.

- [41] Semmah A, Bég OA, Mahmoud SR, Heireche H, Tounsi A. Thermal buckling properties of zigzag single-walled carbon nanotubes using a refined nonlocal model, *Adv. Mats Res*, 2014,3:1-13.
- [42] Uddin MJ, Yusoff NHM, Bég OA, Ismail AIM, Lie group analysis and numerical solutions for non-Newtonian nanofluid flow in a porous medium with internal heat generation, *Phys. Scr.* 2013,87:1-14.
- [43] Uddin MJ, Khan WA, Ismail AIM. Free convection boundary layer flow from a heated upward facing horizontal flat plate embedded in a porous medium filled by a nanofluid with convective boundary condition, *Trans in Porous Med* 2012, 92:867-881.
- [44] Arifin NM, Nazar R, Pop I. Similarity solution of Marangoni convection boundary layer flow over a flat surface in a nanofluid, *J Applied Math* 2013, 2013, Article ID 634746, 8 pages.
- [45] Bég OA, Zueco J, Bég TA, Takhar HS, Kahya E. NSM analysis of time-dependent nonlinear buoyancy-driven double-diffusive radiative convection flow in non-Darcy geological porous media. *Acta Mech* 2009; 202:181-204.
- [46] Bég OA, Motsa SS. M.N. Islam and M. Lockwood, Pseudo-spectral numerical analysis of exothermically-reacting Rivlin-Ericksen viscoelastic flow and heat transfer in a rocket propulsion duct. *Comput Therm Sci* 2014a; 6: 1-12.
- [47] Bég OA, Zueco J, Norouzi M, Davoodi M, Joneidi AA, Elsayed AF. Network and Nakamura tridiagonal computational simulation of electrically-conducting biopolymer micro-morphic transport phenomena. *Comput in Biology and Med* 2014b; 44:44–56.
- [48] Pal, D., Talukdar, B., Shivakumara, I.S., Vajravelu, K. Effects of Hall current and chemical reaction on oscillatory mixed convection-radiation of a micropolar fluid in a rotating system. *Chem Eng Commun* 2012, 199(8):943-965.
- [49] R. Viskanta, Radiation heat transfer in materials processing and manufacturing, *Energy and the Environment*, 1999, 15:101-112.

Figures

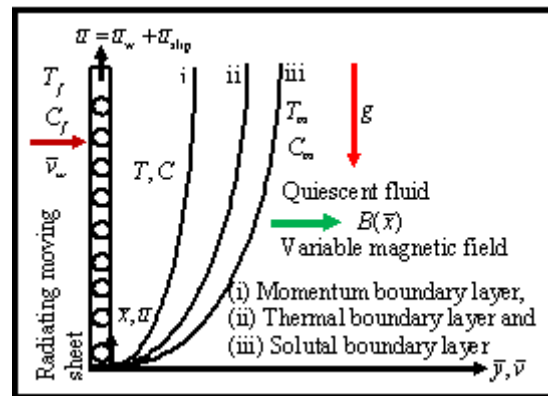


Figure 1: Flow configuration and coordinate system.

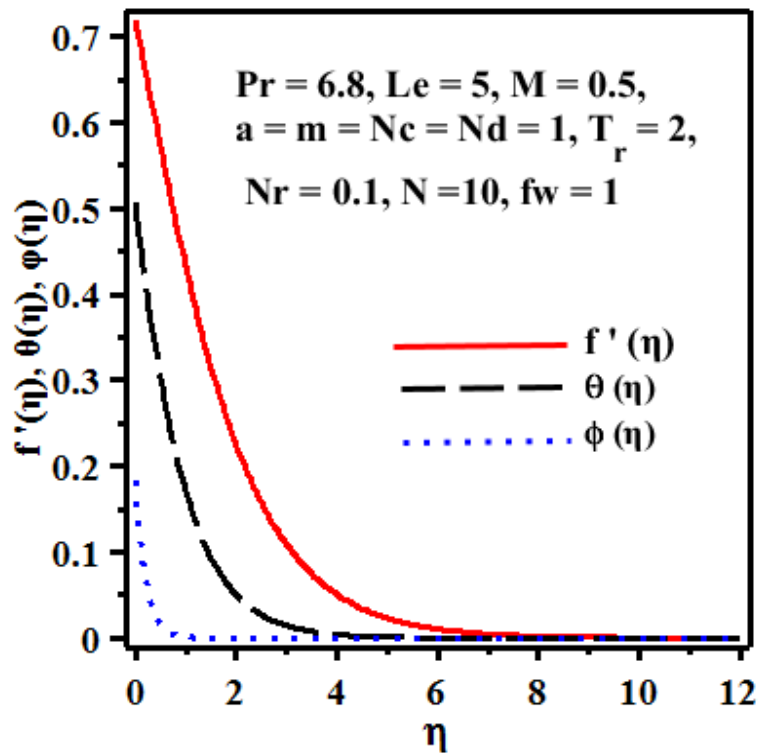


Fig.2 Sample graph of velocity, temperature and concentration.

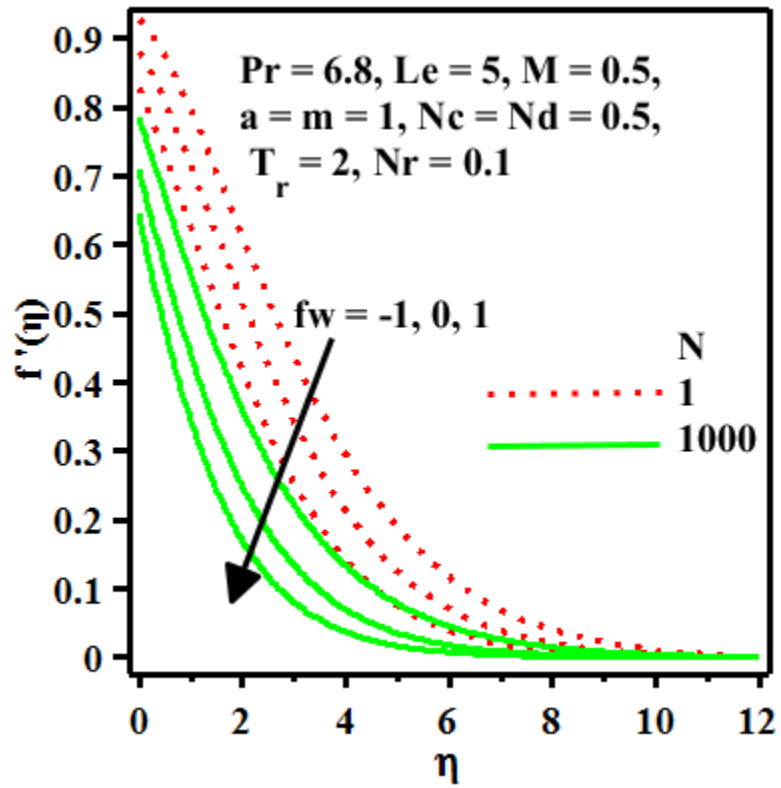


Fig. 3. Effect of N and fw on the velocity distributions.

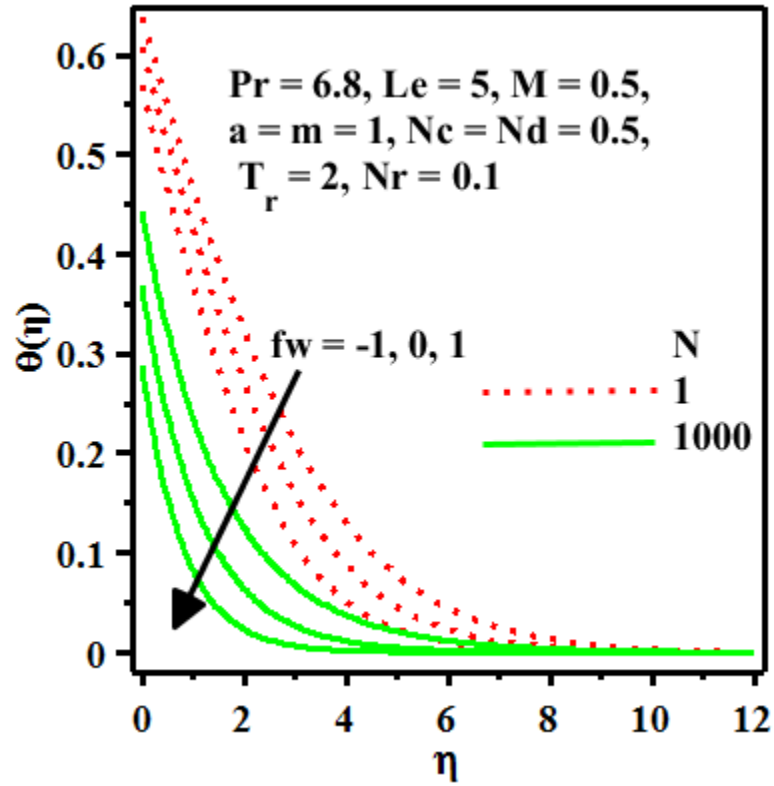


Fig. 4. Effect of N and fw on the temperature distributions.

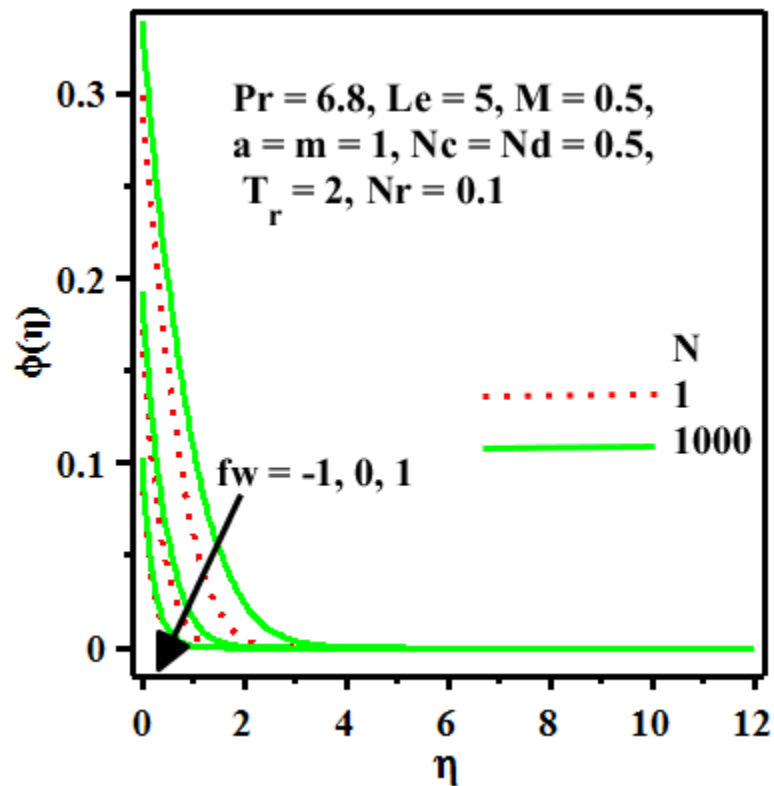


Fig. 5. Effect of N and fw on the concentration distributions.

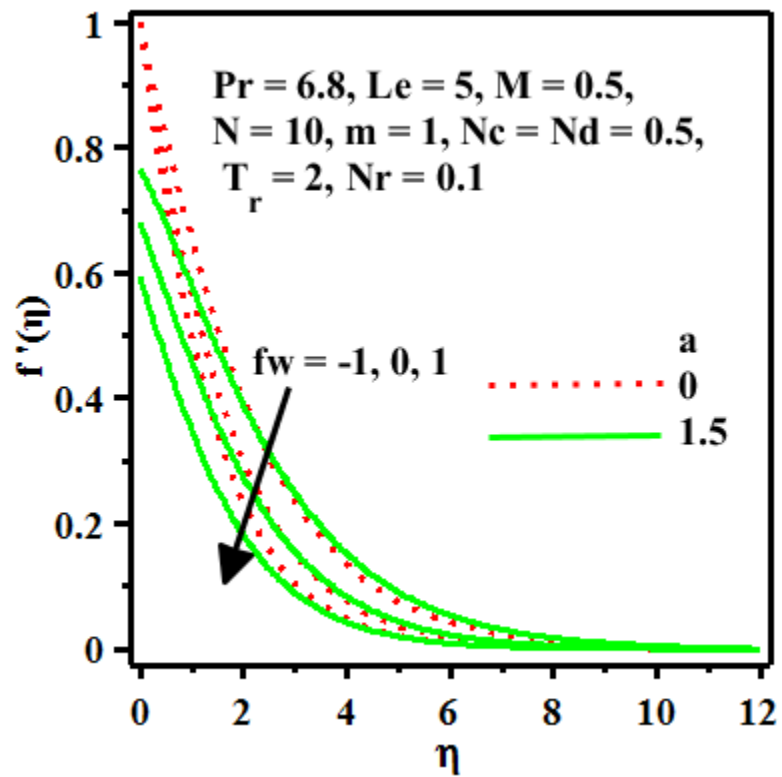


Fig. 6. Effect of a and fw on the velocity distributions.

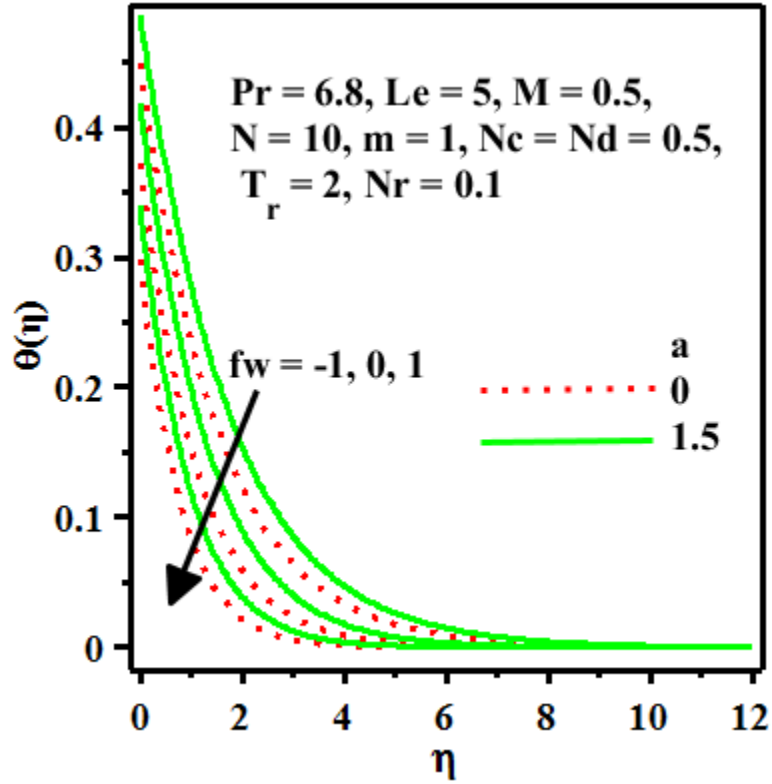


Fig. 7. Effect of a and fw on the temperature distributions.

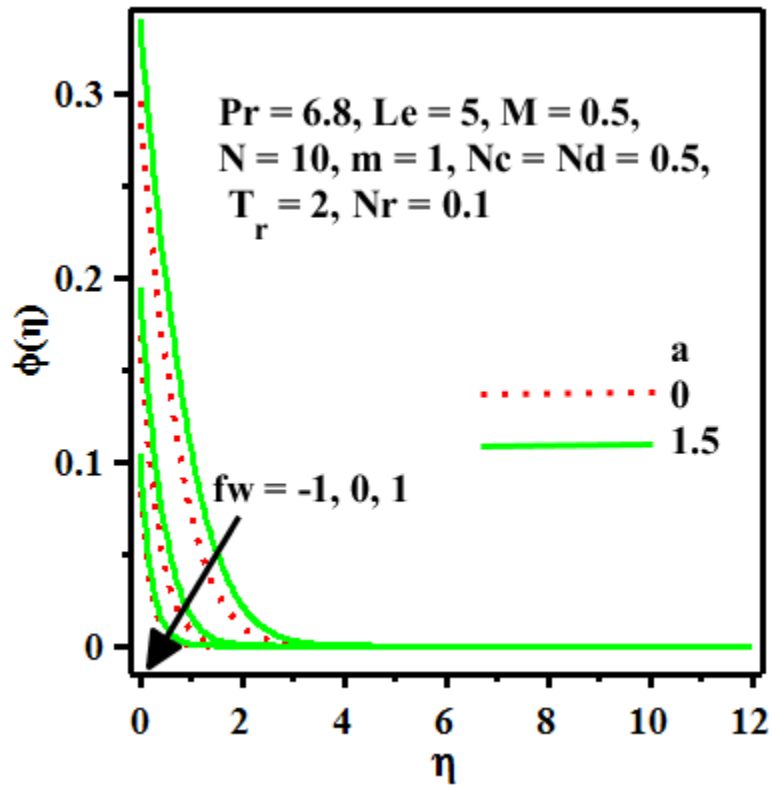


Fig.8. Effect of a and fw on the concentration distributions.

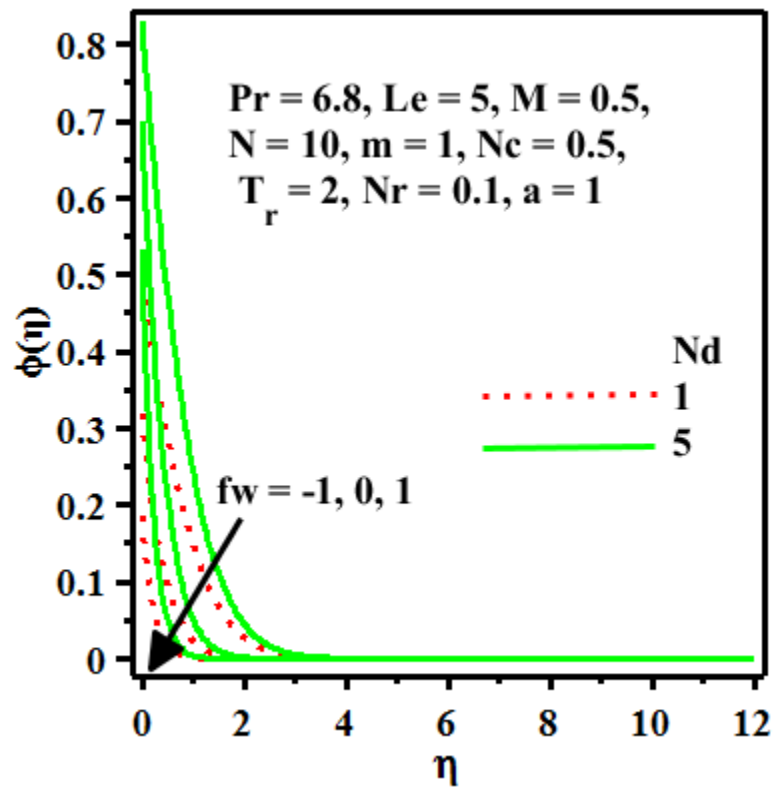


Fig. 9. Effect of Nd and fw on the concentration distributions.

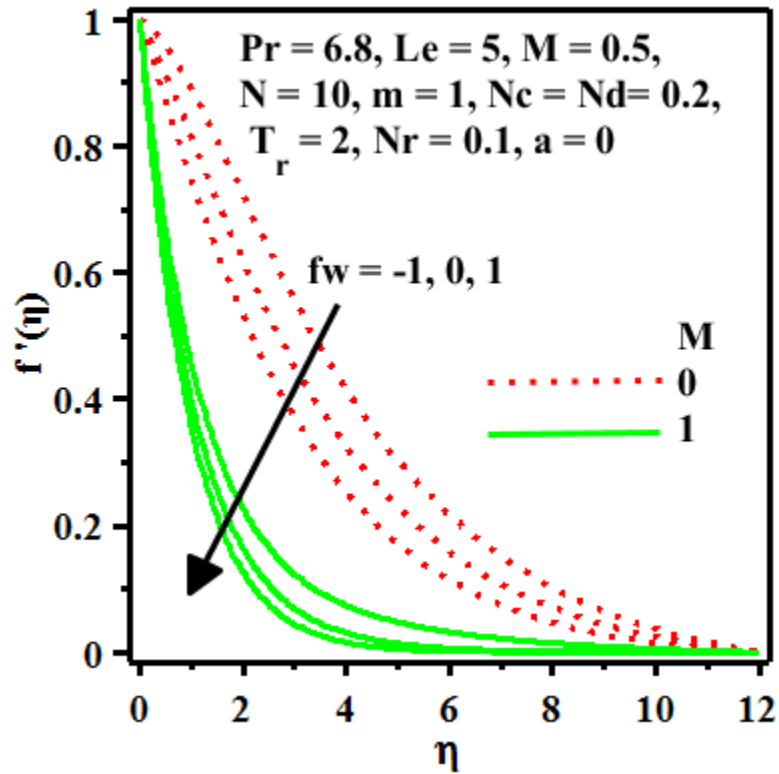


Fig. 10. Effect of M and fw on the temperature distributions.

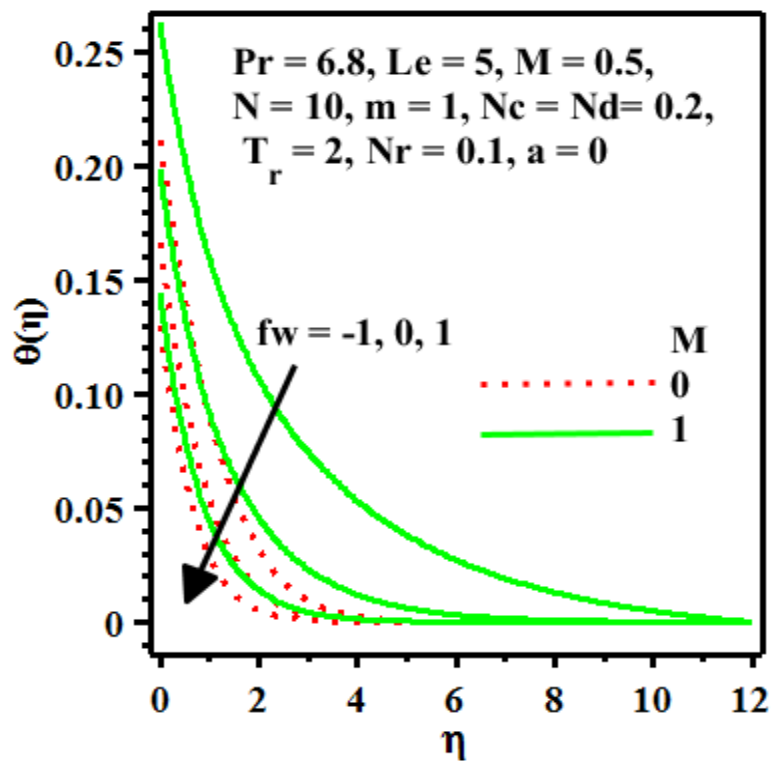


Fig. 11. Effect of M and fw on the temperature distributions.

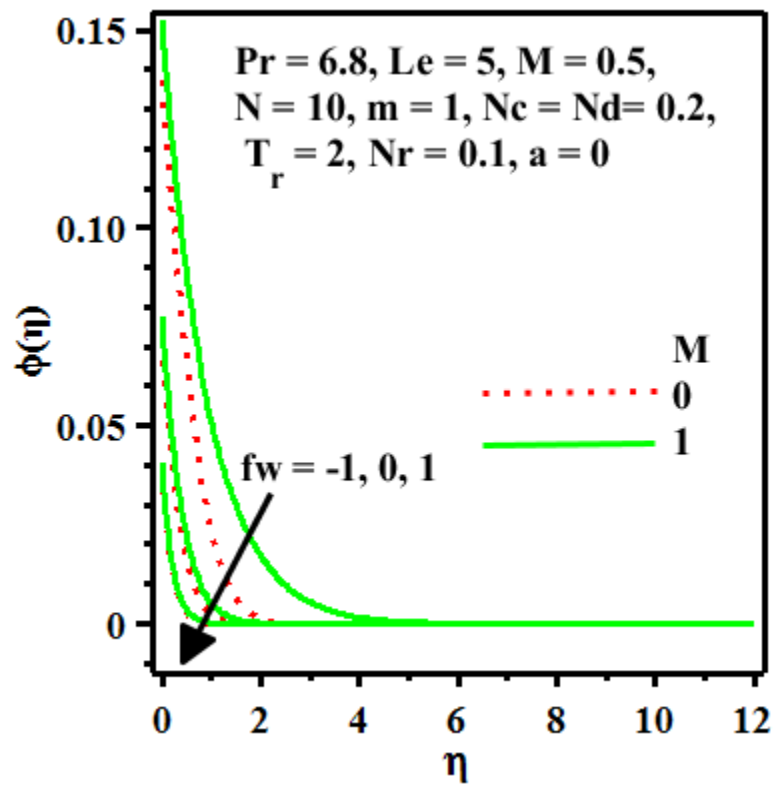


Fig. 12. Effect of M and fw on the concentration distributions.

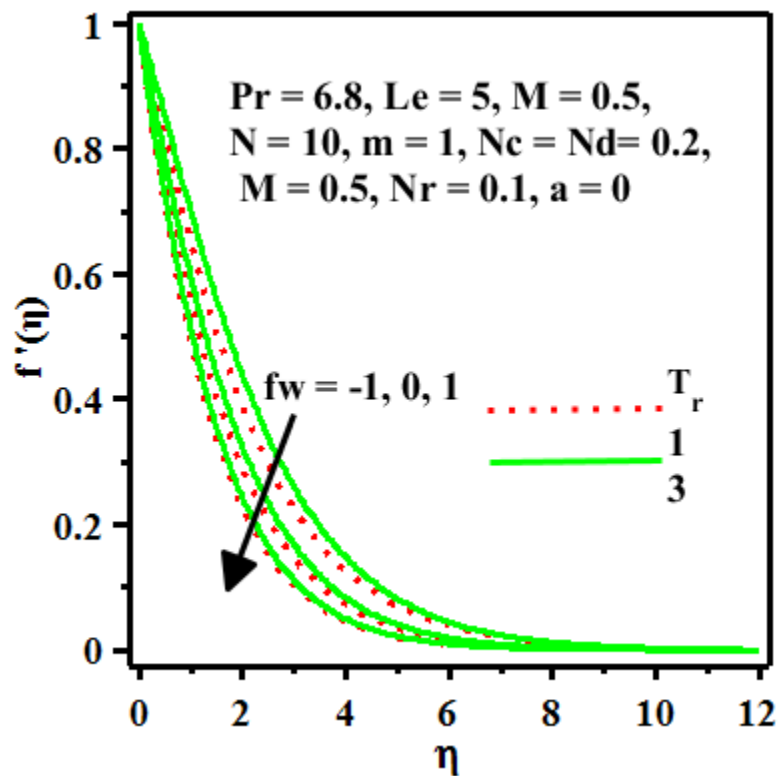


Fig. 13. Effect of T_r and fw on the velocity distributions.

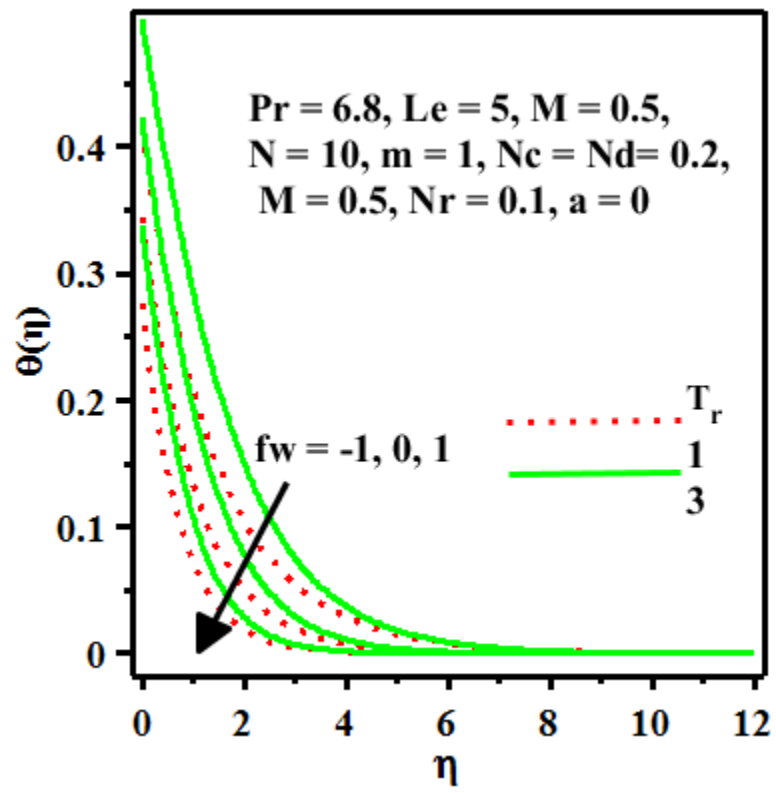


Fig. 14. Effect of T_r and fw on the temperature distributions.

Tables

Table 1

Comparison of values of $f''(0)$ for several suction/injection parameter fw .

fw	$f''(0)$	
	Cortell [24]	Present results
-0.75	0.984417	0.984439
-0.50	0.873627	0.873643
0	0.677647	0.677648
-0.50	0.518869	0.518869
-0.75	0.453521	0.453523

Table 2

Values of $f''(0)$, $-\theta'(0)$ and $-\phi'(0)$ when $Pr = 6.8, Le = 5, m = 1, Nr = fw = 0.1$.

M	a	Nc	Nd	N	Tr	$-f''(0)$	$-\theta'(0)$	$-\phi'(0)$
0	0.1	0.1	0.1	10	2	0.20026	0.09123	0.09647
0.5	0.1	0.1	0.1	10	2	0.93573	0.08993	0.09623
1	0.1	0.1	0.1	10	2	0.88003	0.08899	0.09609
0.1	0.5	0.1	0.1	10	2	0.27768	0.09040	0.09621
0.1	1	0.1	0.1	10	2	0.22889	0.09603	0.08992
0.1	0.1	0.5	0.1	10	2	0.17693	0.09647	0.32727
0.1	0.1	1	0.1	10	2	0.06352	0.47308	0.09652
0.1	0.1	0.1	0.5	10	2	0.33178	0.09089	0.42137
0.1	0.1	0.1	1	10	2	0.33178	0.09089	0.42137
0.1	0.1	0.1	0.1	50	2	0.34145	0.09148	0.09639
0.1	0.1	0.1	0.1	100	2	0.34225	0.09155	0.09639
0.1	0.1	0.1	0.1	10	2.5	0.33394	0.09077	0.09640
0.1	0.1	0.1	0.1	10	3	0.33276	0.09064	0.09640